Investigation of heat transfer characteristics in the developing and the developed flow of nanofluid inside a tube with different entrances in the transition regime

Masoud Jamali[1] · Davood Toghraie[1]

Abstract

In this paper, we studied heat transfer characteristics in the developing and the developed flow of nanofluid inside a tube with different entrances in the transition regime. A range of Reynolds numbers from $Re = 500$ to 13,000 was stimulated to examine flow characteristics in the tube. Effect of entrance, diameter of nanoparticles, nanoparticle type, Reynolds number and concentration of nanoparticles on onset of transition were studied. The results show that heat transfer coefficient and Nusselt number of base fluid and the nanofluid increase with increasing Reynolds number. Also, convective heat transfer coefficient of nanofluid increases by increasing Reynolds number, and the rate of increase in heat transfer coefficient varies depending on diameter, volume fraction and type of nanoparticles. Furthermore, the results show that local Nusselt number and local convective heat transfer coefficient slightly decrease with increasing particle diameter at constant volume fraction of nanoparticles.

Introduction

Numerous works have revealed that the extent of the amplification region and hence the location of the transition point on the body surface are strongly dependent not only upon the amplitude and/or the spectrum of external disturbances but also on their physical nature. Some of the disturbances easily penetrate into the boundary layer, while others do not. Consequently, the concept of boundary layer transition is a complex one and still lacks a complete theoretical exposition [1]. A nanofluid is a fluid containing nanoparticles. They exhibit enhanced thermal conductivity and the convective heat transfer coefficient compared to the base fluid. The previous works show that the proportional increase in pressure drop for turbulent flow is higher than that for laminar flow as the base fluid. Also, there is no significant increase in pressure drop at laminar flow. An

optimum concentration must be found for each nanofluid system in which more heat transfer enhancement and less flow resistance occur in different flow regimes. In the transition regime, the experiments were performed on the heating of the fluid, except for those conducted by Manglik and Bergles [2], who also investigated the flow in the transition region by means of the cooling of the fluid. Most of the augmentation techniques involved the inserts of tapes [2] and wire coils [3, 4]. No helical finned-type tubes have yet been tested in this region. The fluids used were a mixture of water and ethylene/propylene glycol. Tam and Ghajar [5] investigated transitional heat transfer in plain horizontal tubes. They presented a flow regime map for determination of the boundary between forced and mixed convections in horizontal tubes with different inlets. Chong et al. [6] investigated the effects of duct inclination angle on thermal entrance region of laminar and transition mixed convection. They concluded that when Reynolds numbers further increased, the friction factors were almost independent of inclination angles. Celata et al. [7] studied friction factor in micro-pipe gas flow under laminar, transition and turbulent flow regimes. They concluded that the laminar-to-turbulent transition starts for Reynolds number

✉ Davood Toghraie
  Toghraee@iaukhsh.ac.ir

1   Department of Mechanical Engineering, Khomeinishahr Branch, Islamic Azad University, Khomeinishahr, Iran

not lower than 2000 for smooth pipes, while tending to larger values (3200–4500) for rough pipes. Lorenzini et al. [8] investigated laminar, transitional and turbulent friction factors for gas flows in smooth and rough micro-tubes. They observed that the transitional regime was found to start no earlier than at values of the Reynolds number around 1800. Meyer and Olivier [9] studied transitional flow inside enhanced tubes for fully developed and developing flows with different types of inlet disturbances. They found that inlet disturbances had no effect on the critical Reynolds numbers, with transition occurring at a Reynolds number of approximately 2000 and ending at $Re = 3000$. Almohammadi et al. [10] investigated convective heat transfer and pressure drop of Al_2O_3/water nanofluid in laminar flow regime inside a circular tube. They concluded that there is no significant increase in friction factor for nanofluids. Wang et al. [11] studied forced convection heat transfer and flow characteristics in laminar-to-turbulent transition region in rectangular channel. Their results show that the lower and the upper critical Reynolds number of transition region increase with the decrease in Prandtl number. Heyhat et al. [12] investigated the laminar convective heat transfer and pressure drop of water-based Al_2O_3 nanofluids in fully developed flow regime. Tam et al. [13] studied the effect of inlet geometries and heating on the entrance and fully developed friction factor in laminar and transition regions of a horizontal tube. They concluded that the heating condition caused an increase in the lower and upper limits of the isothermal transition boundaries and a decrease in the entrance and fully developed flow apparent friction factors in the laminar and transition regions. Karimzadeh khouei et al. [14] investigated pressure drop and heat transfer characteristics of nanofluids in horizontal microtubes under thermally developing flow conditions. They observed that at low Reynolds numbers, flow is mainly laminar. However, at higher Reynolds numbers, flow starts to transition to turbulent flow. Heris et al. [15] simulated convective heat transfer and pressure drop in laminar flow of Al_2O_3/water and CuO/water nanofluids through square and triangular cross-sectional ducts. They observed that heat transfer coefficient of nanofluid increases in comparison with heat transfer coefficient of pure water. Their results show that by adding nanoparticles, pressure drop increases in ducts. Li et al. [16] investigated the heat transfer and pressure drop of ZnO/ethylene glycol–water nanofluids in transition flow. Their measurements showed that the pressure drop of nanofluid was higher than that of the base fluid in a turbulent flow regime.

The objective of this paper is to investigate the heat transfer characteristics in the developing and the developed flow of nanofluid inside a tube with different entrances in the transition regime. Heat transfer coefficient of nanofluid

flow and effective parameters in transition flow at $Re = 2100$ to 3100 were studied in the tube without inlet and a smooth tube. Heat transfer coefficient and Nusselt number of base fluid and the nanofluid are investigated by increasing the Reynolds number and volume fraction of nanoparticles.

Geometry of the problem

The schematic of the tube without inlet is shown in Fig. 1, and the schematic of the tube with inlet is shown in Fig. 2. For the tube without inlet, water enters a 7.4-m-long and 8.14-mm-thick tube at the temperature of 40 °C and $Re = 13,000$. The first 2.4 m was adiabatic, and a fixed temperature of 20 °C was applied on the wall in the final 5 m of the tube where flow has become developed. For the tube with inlet, water enters the 140-mm-thick tube at 40 °C and $Re = 1280$ and then enters the main 8.14-mm-thick tube with a fixed temperature of 20 °C on the walls. The meshing for the tube without inlet is shown in Fig. 3a, and the meshing for the tube with inlet is shown in Fig. 3b. The dimensions of these tubes are presented in Table 1.

Governing equations

Conservation equations

For a steady, incompressible, axisymmetric flow inside a circular tube with different entrances, the conservation equations of mass, momentum and energy are expressed as follows:

Continuity equation

$$\text{div}(\rho_{nf} \overrightarrow{V}) = 0 \tag{1}$$

Conservation of momentum

$$\text{div}(\rho_{nf} \overrightarrow{V}\, \overrightarrow{V}) = -\overrightarrow{\nabla}P + \nabla \cdot (\mu_{nf} \nabla \overrightarrow{V}) \tag{2}$$
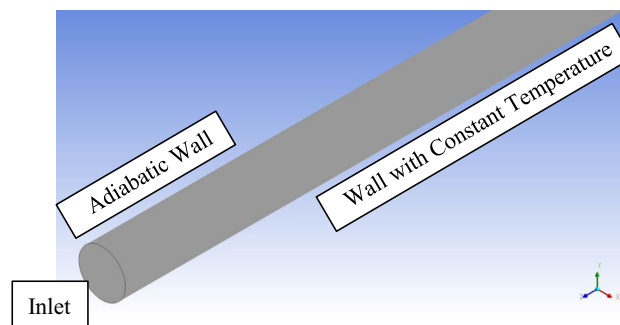
Conservation of energy
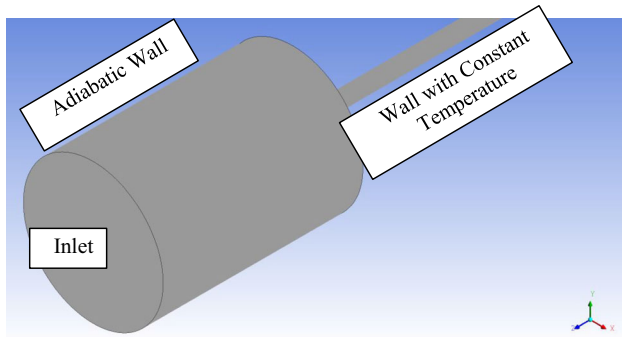

Fig. 1 Schematic of the tube without inlet

Fig. 2 Schematic of the tube with inlet

$$\text{div}(\rho_{nf}\overrightarrow{V}C_{p,nf}T) = \text{div}(k_{nf}\ \text{grad}T) \tag{3}$$

where $\overrightarrow{V}$, P and T are velocity vector, pressure and temperature, respectively.

Thermal properties of the base fluid

Pure water was selected as the base fluid. The physical properties of water are the functions of temperature. According to [17], water viscosity is given by Eq. 4. Thermal conductivity, density and specific heat are given by Eqs. 5–7, respectively,

$$\mu_{bf} = 0.00002414 \times 10^{(247.8/(T-140))} \tag{4}$$

$$\begin{aligned} k_{bf} = {} & 2.33417 - 0.0328575T + 0.000185702T^2 \\ & - 4.18409 \times 10^{-7}T^3 + 3.33928 \times 10^{-10}T^4 \end{aligned} \tag{5}$$

$$\begin{aligned} \rho_{bf} = {} & -598.113 + 17.5482T - 0.0708339T^2 \\ & + 0.00012660T^3 - 8.80307 \times 10^{-8}T^4 \end{aligned} \tag{6}$$

$$\begin{aligned} C_{Pbf} = {} & -29664.8 + 403.224T - 1.78895T^2 \\ & + 0.00349982T^3 - 0.00000254434T^4 \end{aligned} \tag{7}$$

The relations are true in the temperature range $293K \le T \le 363K$.

Properties of nanofluid

In order to calculate the density and specific heat, Eqs. 8 and 9 are used, respectively [18, 19],

$$\rho_{nf} = (1-\varphi)\rho_{bf} + \varphi\rho_p \tag{8}$$

$$C_{pnf} = \frac{\varphi\rho_p C_{P_p} + (1-\varphi)\rho_{bf}C_{pbf}}{\rho_{nf}} \tag{9}$$

Viscosity is calculated by using Eqs. 10 and 11 [20, 21], and thermal conductivity is calculated from Eqs. 12–15 [22],

$$\frac{\mu_{nf}}{\mu_{bf}} = 1 + 11\varphi \qquad \text{(Water/CuO)} \tag{10}$$

$$\frac{\mu_{nf}}{\mu_{bf}} = 1 + 1631\left(\frac{\varphi}{1-\varphi}\right)^{2.8} \qquad \text{(Alumina/Water)} \tag{11}$$

$$k_{nf} = \frac{(k_p + 2k_{bf} - 2(k_{bf} - k_p)\varphi)}{(k_p + 2k_{bf} + (k_{bf} - k_p)\varphi)}k_{bf} \tag{12}$$

Alumina and CuO nanoparticles were used in this research. The properties of these nanoparticles are represented in Table 2 [23].

Boundary conditions

A steady and incompressible flow (pure or nanofluid) with uniform velocity profile enters the tube (with and without inlet) at 30 °C and exits the tube with constant pressure (pressure outlet). Constant and uniform temperature of 50 °C was selected as boundary condition on the tube. Fluid is discharged to the environment exiting the tube.

Numerical method

Local convective heat transfer coefficient is calculated from Eq. 16, and local Nusselt number is calculated from Eq. 14,

$$h(x) = \frac{q''}{T_w - T_b} \tag{13}$$

$$Nu(x) = \frac{h(x)D}{k_{nf}} \tag{14}$$

where q'' represents heat flux, T_w and T_b are, respectively, wall temperature and fluid bulk temperature at distance x from the inlet of the tube, D represents tube diameter and k is thermal conductivity of the fluid which is calculated at T_b. Then, according to Eq. 15, by integrating from local heat transfer coefficient, the average heat transfer coefficient is obtained. Average Nusselt number is obtained from Eq. 16,

$$h_{avg} = \frac{1}{L}\int_0^L h(x)\mathrm{d}x \tag{15}$$

$$Nu_{avg} = \frac{h_{avg}D}{k} \tag{16}$$

Finite volume method (FVM) was employed to solve the equations. The pressure-based solver was employed for coupling the equations. The second-order UPWIND method was used for interpolating the transfer equation. The SIMPLE algorithm was used for pressure–velocity coupling.
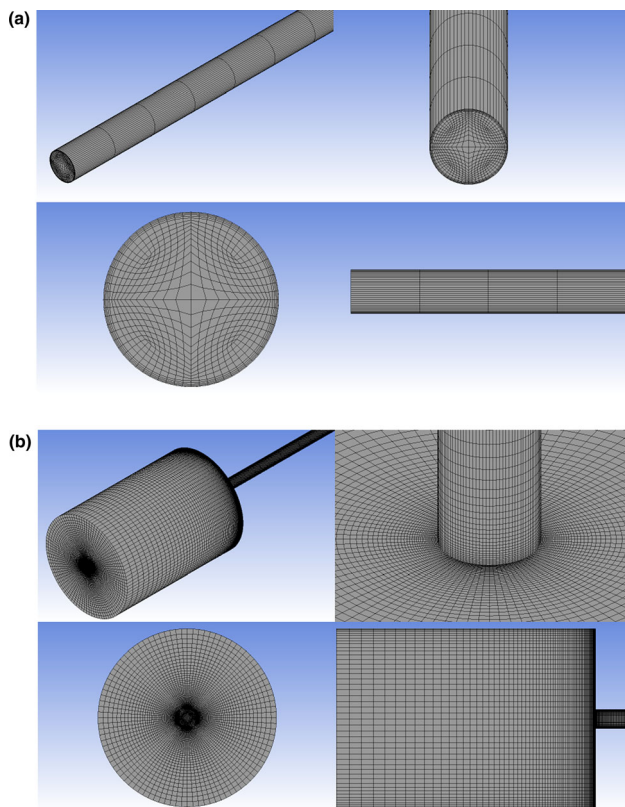
Fig. 3 **a** Meshing for the tube without inlet and **b** meshing for the tube with inlet

Grid independency

In order to verify the sensitivity of grid to the boundary condition, how to change the profile of the axial velocity and the temperature profile in the pipe is evaluated by increasing the number of elements. Axial velocity profiles and temperature profiles at the pipe outlet are drawn at different element numbers in Fig. 4. For the tube without inlet, the grid having 38,400 elements being the most adequate since further refining does not significantly change the velocity and temperature profiles. But for the tube with inlet, meshing with 1,164,384 elements is

appropriate and further refining the grid would not impose any significant changes.

Results and discussion

Validation

Flow of the base fluid (water) in incompressible-to-turbulent regimes from $Re = 500$ to 13,000 was assumed in an adiabatic 4.7-m-long and 88.15-mm-thick tube without inlet. Changes in friction factor in developed region were compared to [24] as shown in Fig. 5. Moreover, the results reported by Kim et al. [25] were used in order to examine nanofluid modeling results. The incompressible flow of water/alumina (3 vol%) nanofluid in a 2-m-long and 57.4-mm-thick tube was modeled under constant heat flux and at $Re = 1460$. Results are presented in Fig. 6.

Developed flow in a smooth tube

A range of $Re = 500$ to 13,000 was stimulated in transition from laminar flow to turbulent flow to examine the flow in the tube. The entrance length of tube was intended as 2.4 m for fully developed flow. The effect of tube diameter on onset of transition was studied in water/alumina nanofluid at 2% volume fraction by using friction factor. Figures 7 and 8 show the friction factor for two tubes (with different diameters) with water/alumina nanofluid with 2% volume fraction. The results for the two tubes are consistent with the analytical results. Transition zone is magnified in Fig. 8. The results show that flow transition starts at $Re = 2100$ to 2300 and ends at $Re = 3100$ in the smooth tube without inlet. Friction factor increases at the onset of transition. The results show that the addition of nanoparticles does not affect the onset of transition.

The effect of inlet on onset of transition

In this section, the effect of tube diameter and inlet shape on onset of transition is assessed using adiabatic friction

Table 1 Dimensions of the tubes used in this simulation

	Diameter of inlet/mm	Length of inlet/m	Diameter/mm	Length/m
Tube without inlet	14.8	2.4	14.8	5
Tube without inlet	17.7	2.4	17.7	5
Tube with inlet	140	2.4	14.8	5

Table 2 Properties of alumina and CuO nanoparticles [23]

Nanoparticle type	Density/kg/m^{-3}	Specific heat/J kg^{-1} K	Thermal conductivity/W mK^{-1}
Alumina (Al$_2$O$_3$)	3600	765	36
CuO (CuO)	6500	533	65.17

factor of water fluid and water/alumina nanofluid at 2% volume fraction for two different inlet shapes. Transition from laminar flow to turbulent flow occurs at different Reynolds numbers by modifying the tube inlet shape. An inlet prior to the tube postpones transition at $Re = 2100$ to 2800. Moreover, enlargement of the tube diameter had no effect on changing the Reynolds number of transition flow. Figures 9 and 10 show the friction factor versus the Reynolds number for the tube without inlet with 14.8 mm and 17.7 mm diameters and the tube with sharp edge inlet and 14.8 mm diameter. Friction factor of water fluid was also studied at $Re = 1000$ to 13,000. The addition of nanoparticles to the base fluid did not considerably increase or decrease the friction factor. Figures 11 and 12 show the effect of inlet shape and tube diameter on onset of transition flow. Larger is the tube diameter, less delayed the onset of transition flow. Studies were performed in two parts. Transition zone in the tube with and without inlet and

the effect of tube diameter on onset of flow were determined. Friction factor of the tube was tested in the above two parts. Table 3 shows onset of transition zone depending on diameter and inlet shape of the tube.

Convective heat transfer of nanofluid

Effect of Reynolds number

Figure 13 shows major changes in convective heat transfer coefficient and local Nusselt number of water base fluid with respect to Reynolds number. As expected earlier, convective heat transfer increased by increasing the Reynolds number due to reduced boundary layer thickness. Figure 14 shows major changes in convective heat transfer coefficient and local Nusselt number of water/alumina nanofluid at different Reynolds number at 1% volume fraction and 35 nm diameter of nanoparticle. Similar to
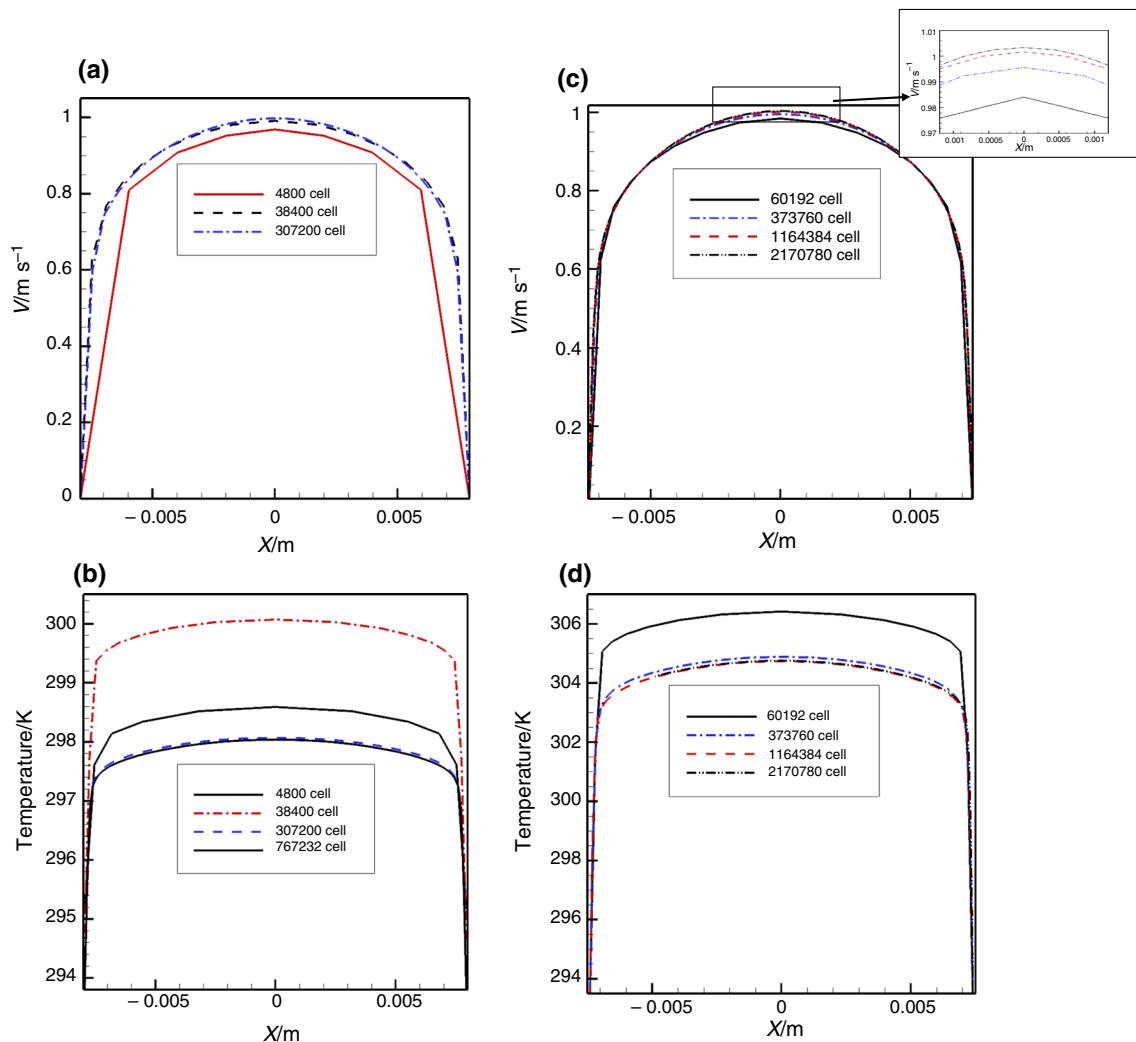

Fig. 4 **a** Axial velocity profile at the pipe outlet without inlet, **b** temperature profile at the pipe outlet without inlet, **c** axial velocity profile at the pipe outlet with inlet, **d** temperature profile at the pipe outlet with inlet
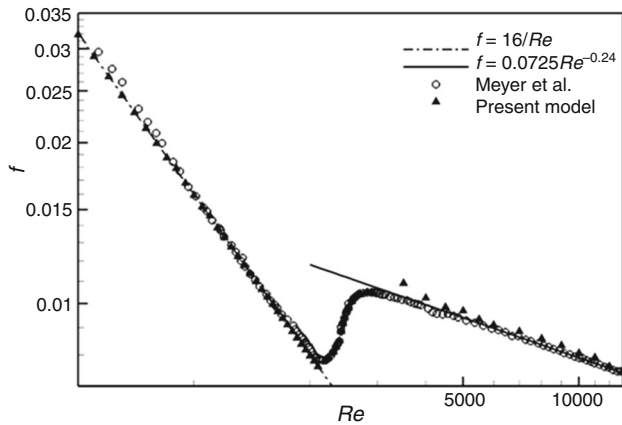
Fig. 5 Friction factor in a 88.15-mm-thick tube, with Meyer et al. [24]
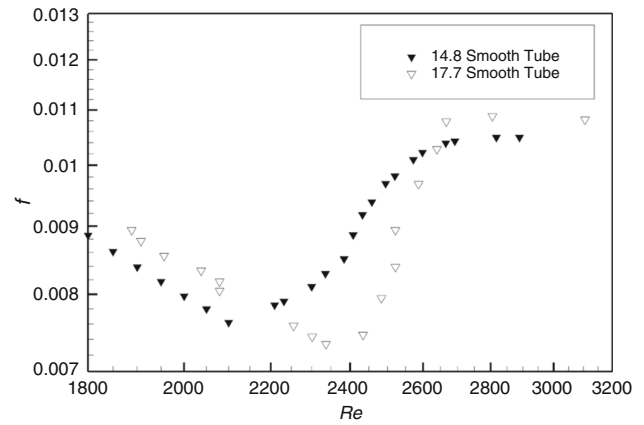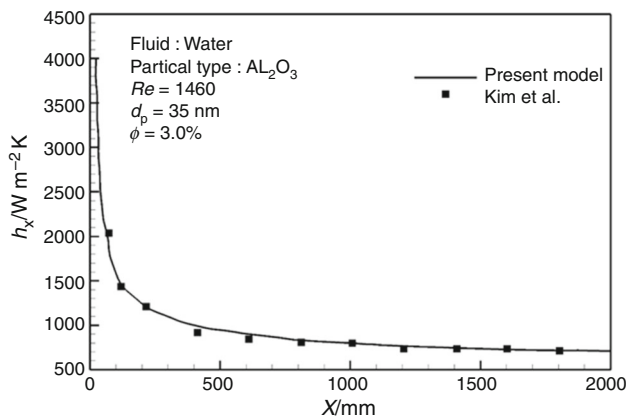

Fig. 6 Local heat transfer coefficient of the water/alumina nanofluid (3 vol%) at $Re = 1460$, with Kim et al. [25]
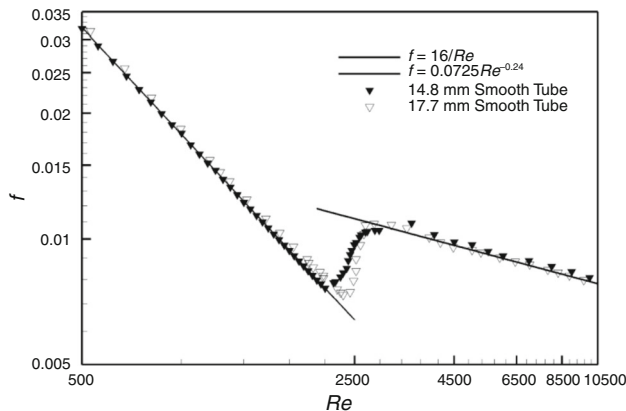

Fig. 7 Friction factor for two tubes with different diameters in water/alumina nanofluid with 2% volume fraction

base fluid, convective heat transfer coefficient increased with increasing Reynolds number.

Similarly, Fig. 15 shows local heat transfer coefficient and local Nusselt number of water/CuO nanofluid at

Fig. 8 Magnification of transition zone for Fig. 11

different Reynolds number at 3% volume fraction and 35 mm diameter of nanoparticle. The same trend was observed in water/CuO nanofluid as water/alumina nanofluid. Convective heat transfer coefficient increased with increasing Reynolds number. Similar charts can be drawn for other concentrations. The same trend can be observed in convective heat transfer coefficient in all charts.

The effect of Reynolds number on the nanofluid flow was studied in local charts in a qualitative manner. Average convective heat transfer coefficient is calculated from Eq. 18 to compare the results more efficiently. Figure 16 shows average convective heat transfer coefficient of water/alumina nanofluid versus Reynolds number in four different volume fractions and 35 nm diameter of nanoparticles. Convective heat transfer coefficient increased by 11% in water fluid at $Re = 2900$ compared to $Re = 2100$. Furthermore, convective heat transfer coefficients increased by 9% and 14.4% at 1% and 4% volume fractions of water/alumina nanofluid. Figure 17 shows average convective heat transfer coefficient of water/CuO
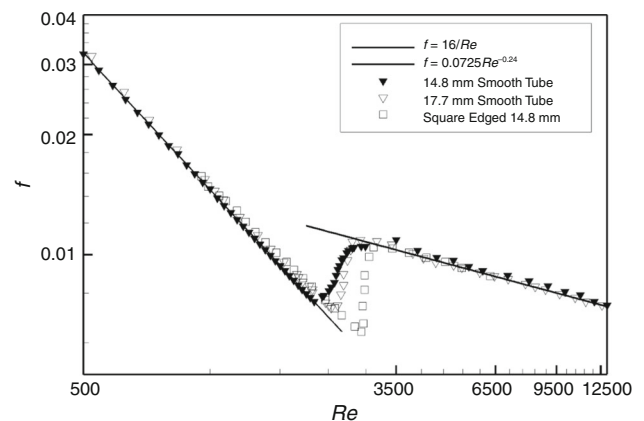

Fig. 9 Friction factor versus Reynolds number for the tube without inlet with 14.8 mm and 17.7 mm diameters and the tube with sharp edge inlet and 14.8 mm diameter
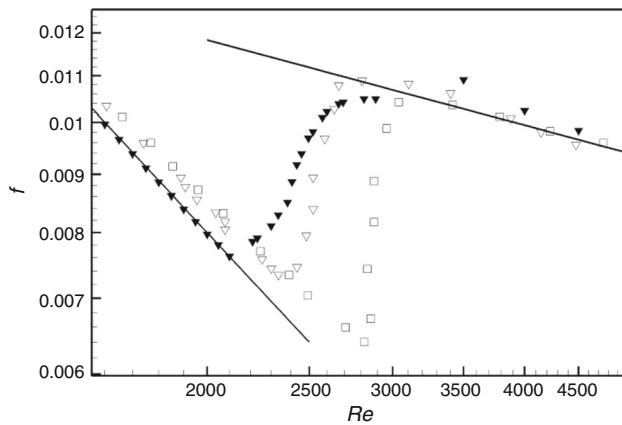
Fig. 10 Magnification of transition zone for Fig. 9

nanofluid versus Reynolds number at four volume fractions and 35 nm diameter of nanoparticles. Convective heat transfer coefficient of CuO nanofluid increased by increasing Reynolds number [26–38]. The same trend was also observed in alumina nanofluid. For example, average heat transfer coefficients increased by 10.8% and 10.6% at 2% and 3% volume fractions by increasing Reynolds number.

Effect of volume fraction of nanoparticles

Volume fraction of particles is another effective parameter in increasing heat transfer rate of nanofluid. Addition of nanoparticles increases the thickness of thermal boundary layer and reduces temperature gradient in vicinity of the wall. On the other hand, thermal conductivity of the nanofluid increased with increasing volume fraction. These two parameters increased the convective heat transfer coefficient in a combined effect. In addition, nanofluid density increased, which increased the momentum and convection heat transfer with increasing volume fraction of
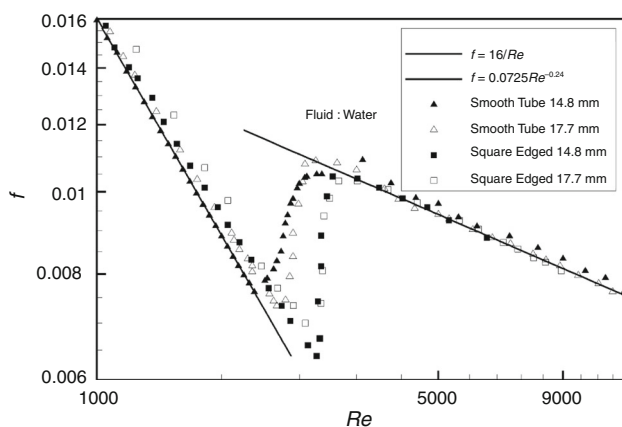

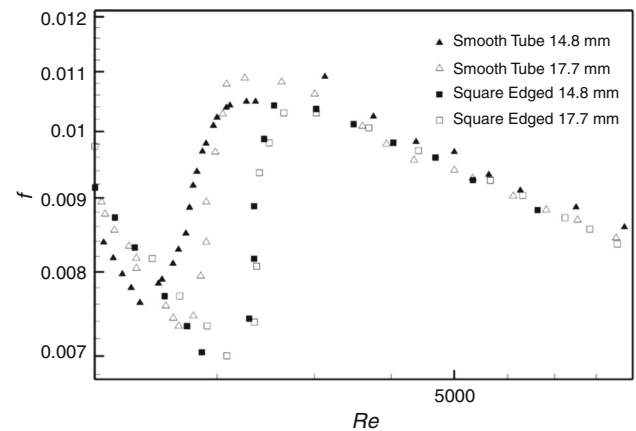**Fig. 11** Effect of inlet shape and tube diameter on onset of transition flow

Fig. 12 Magnification of transition zone for Fig. 11

nanoparticles. Density gradient between the particles and the difference in temperature of fluid are the most important natural mixing elements in the mixtures. Figures 18–20 show the effect of volume fraction on heat transfer coefficient and local Nusselt number of water/alumina nanofluid at Re = 2100, 2500 and 2900.

The results showed that heat transfer coefficient and local Nusselt number of the nanofluid increase at different Reynolds numbers with increasing volume fraction. Volume fraction of nanoparticle, Brownian motion and aspect ratio of nanoparticles increase the heat transfer coefficient. The same trend was also observed in heat transfer coefficient by increasing Reynolds number. Particle size, particle volume fraction, temperature, properties of the base fluid and nanoparticles are effective in Brownian motion. The results showed that volume fraction, Brownian motion and aspect ratio of nanoparticle increase the heat transfer coefficient. Heat transfer properties of the nanofluid are strongly influenced by the type of base fluid and nanoparticle. Increase in thermal conductivity is not the only reason that improves convection heat transfer of the nanofluid. On the other hand, thermal conductivity model that takes into account the effect of Brownian motion of nanoparticles more accurately predicts the heat transfer coefficient.

Figures 21–23 show the effect of volume fraction on heat transfer coefficient and local Nusselt number of water/CuO nanofluid at Re = 2100, 2500 and 2900. Similarly, the results indicated that convective heat transfer coefficient and local Nusselt number of the nanofluid increased by increasing Reynolds number and various types and diameters of nanoparticles with increasing volume fraction of nanoparticles. It should be noted that the rate of increase varies depending on diameter and type of nanoparticle. CuO has a lower thermal conductivity than alumina. Therefore, thermal conductivity and local Nusselt number increased less in case of water/CuO nanofluid compared to

Table 3 Onset of transition zone depending on diameter and inlet shape of the tube for water/ alumina nanofluid at 2% volume fraction

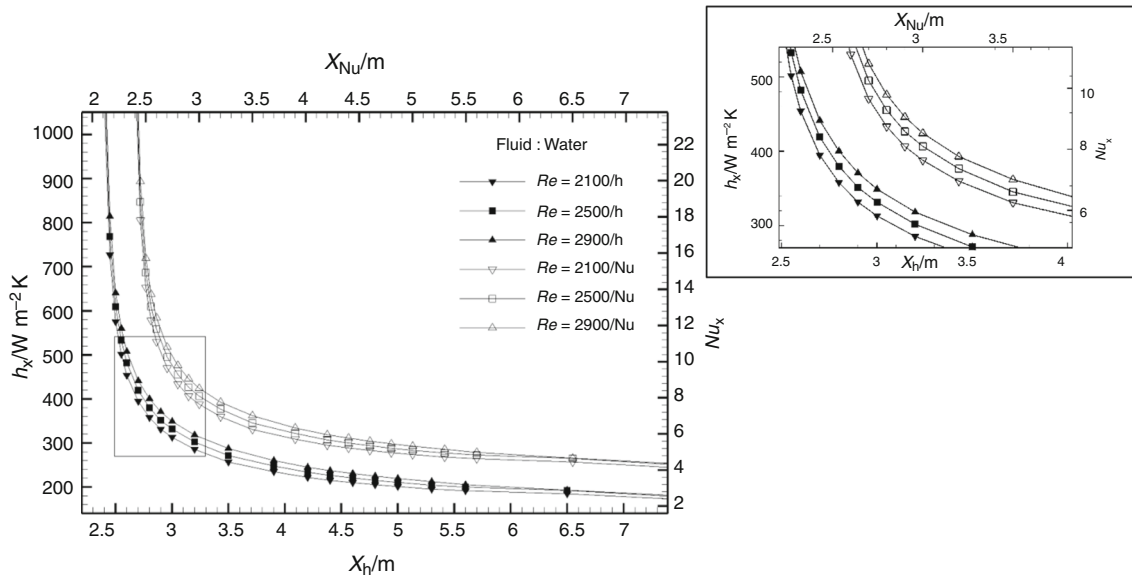| Geometry	Onset of transition	End of transition
Tube without inlet with 14.8 mm diameter	2100	2800
Tube without inlet with 17.7 mm diameter	2300	2800
Tube with inlet with 14.8 mm diameter	2800	3400

Fig. 13 Heat transfer coefficient and local Nusselt number of water base fluid versus Reynolds number
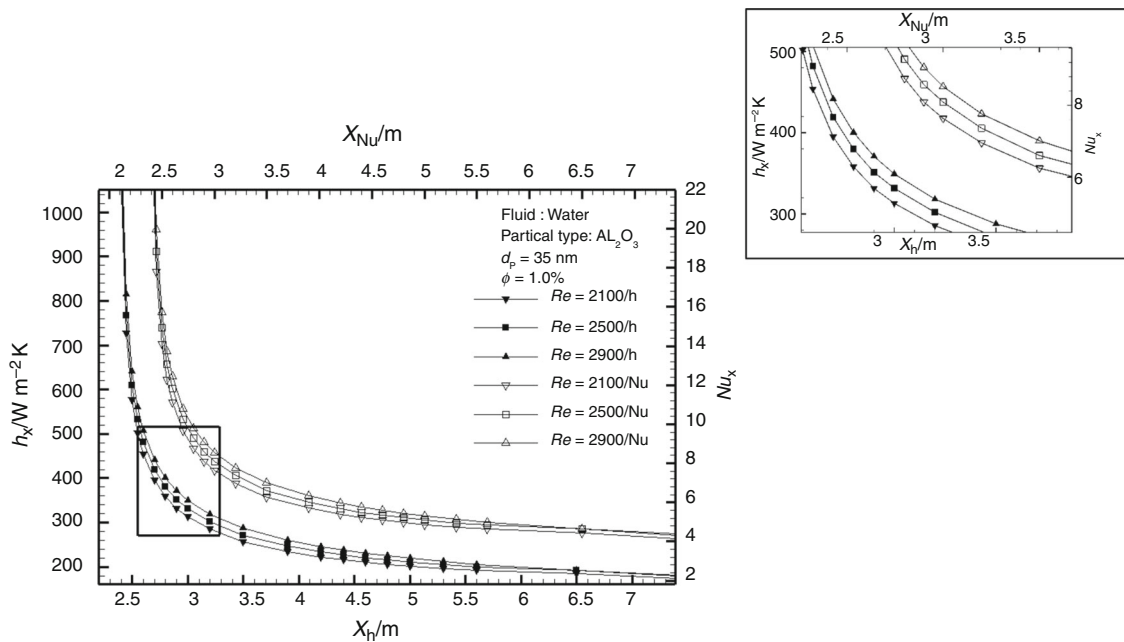

Fig. 14 Local heat transfer coefficient and local Nusselt number of water/alumina nanofluid at different Reynolds number at 1% volume fraction and 35 nm diameter of nanoparticle

water/alumina nanofluid. Moreover, thermal conductivity and local Nusselt number increased less in case of water/ CuO nanofluid by increasing the Reynolds number.

Furthermore, increase in volume fraction of nanoparticles less increased thermal conductivity and Nusselt number in case of water/CuO nanofluid compared to water/alumina
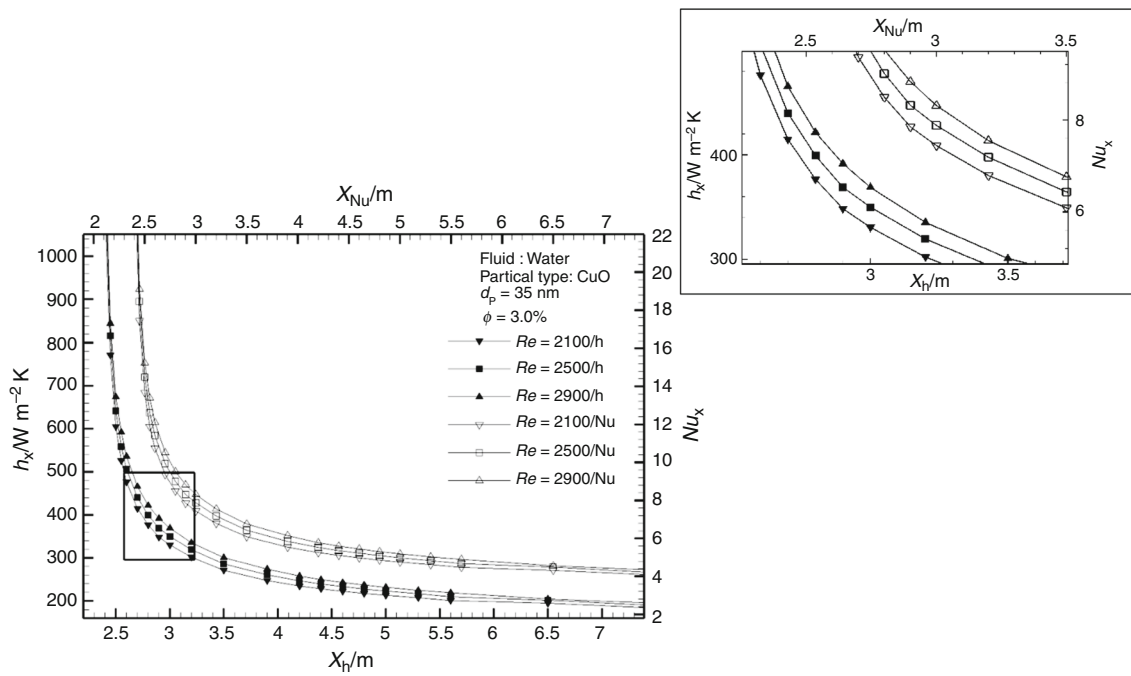
Fig. 15 Convective heat transfer coefficient and local Nusselt number of water/CuO nanofluid with respect to Reynolds number at 3% volume fraction and 35 mm diameter of nanoparticles
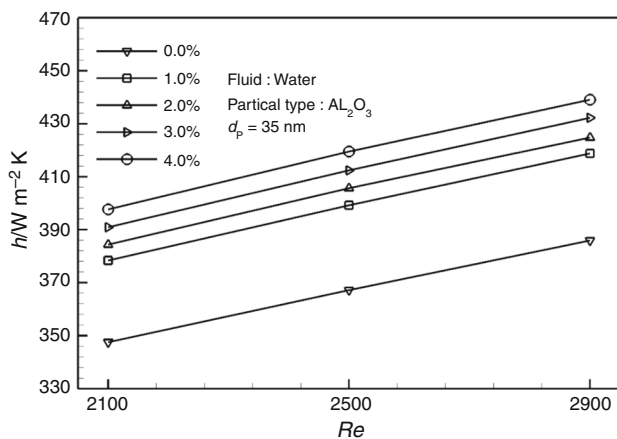

Fig. 16 Average convective heat transfer coefficient of water/alumina nanofluid versus Reynolds number in four different volume fractions and 35 nm diameter of nanoparticles
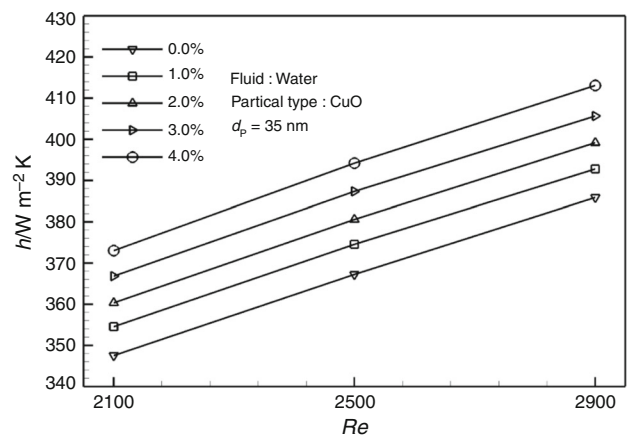

Fig. 17 Average convective heat transfer coefficient of water/CuO nanofluid versus Reynolds number at four volume fractions and 35 nm diameter of nanoparticles

nanofluid due to lower thermal conductivity of CuO compared to alumina.

Figure 24 shows changes in average convective heat transfer coefficient of water/CuO nanofluid and water/alumina nanofluid based on volume fraction of nanoparticles at 35 nm diameter and Re = 2100, 2500 and 2900. The figure shows that average heat transfer coefficient increases by increasing the volume fraction in a given Reynolds number. For example, average heat transfer coefficient increased by 14.4% compared to the base fluid at Re = 2100 and 4% volume fraction of alumina nanoparticles.

Convective heat transfer coefficients increased by 14.2% and 13.75% at Re = 2500 and 2900, respectively. The same upward trend was observed in CuO nanoparticles with increasing volume fraction of particles. For example, convective heat transfer coefficients increased by 7.3%, 7.3% and 7% at Re = 2100, 2500 and 2900 at 4% concentration compared to the base fluid. Non-uniform increase in convective heat transfer coefficient is considerably important. A uniform increase was observed in convective heat transfer coefficient with increasing volume fraction of nanoparticles at Re = 2100 and 2500 in water/
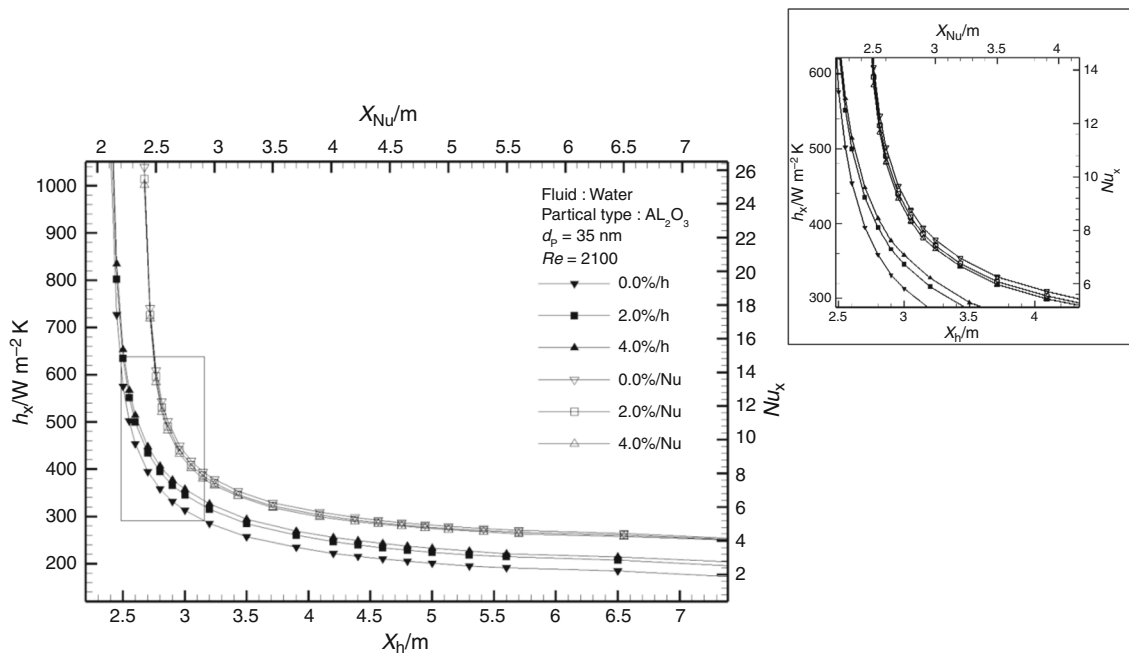
Fig. 18 Effect of volume fraction on heat transfer coefficient and local Nusselt number of water/alumina nanofluid at $Re = 2100$
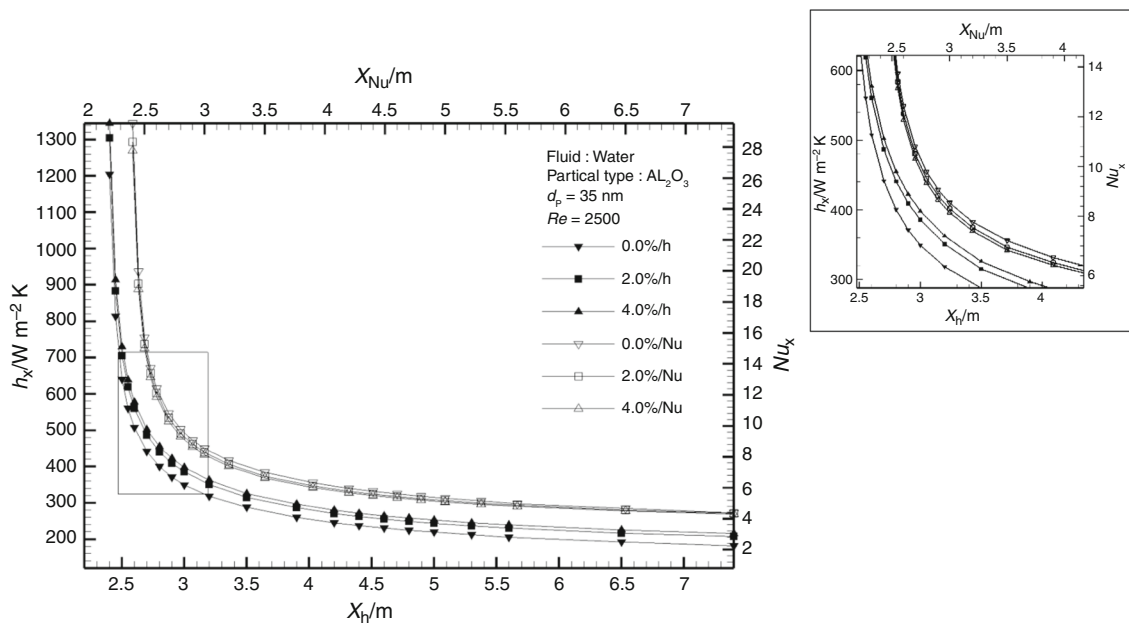

Fig. 19 Effect of volume fraction on heat transfer coefficient and local Nusselt number of water/alumina nanofluid at $Re = 2500$

CuO nanofluid. The difference in volume fraction from 0 to 1% varies from other volume fractions at $Re = 2900$. A sharp increase was observed in convective heat transfer coefficient of water/alumina nanofluid from 0% volume fraction to higher volume fractions. The difference in this coefficient between water/alumina and water/CuO nanofluids is due to higher thermal conductivity of water/alumina nanofluid compared to water/CuO nanofluid. This

results in higher heat transfer coefficient of water/alumina nanofluid compared to water/CuO nanofluid.

The effect of diameter of nanoparticles

Diameter of nanoparticles is another effective parameter in convective heat transfer coefficient of nanofluids. With regard to thermal conductivity equation, diameter of nanoparticles has a negative effect on thermal conductivity
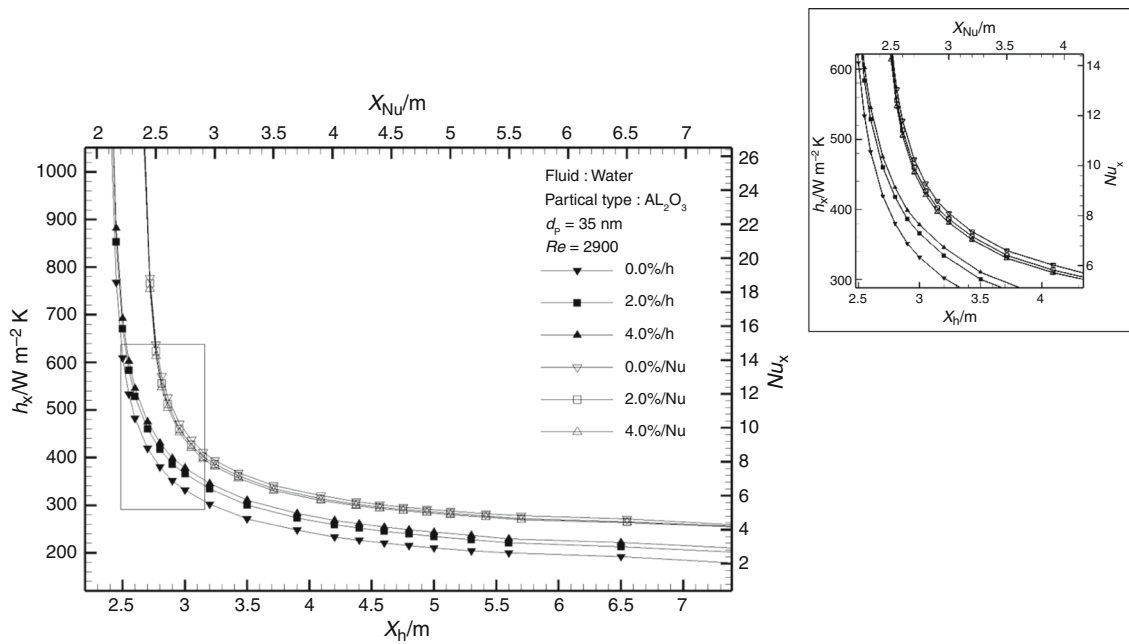
Fig. 20 Effect of volume fraction on heat transfer coefficient and local Nusselt number of water/alumina nanofluid at $Re = 2900$
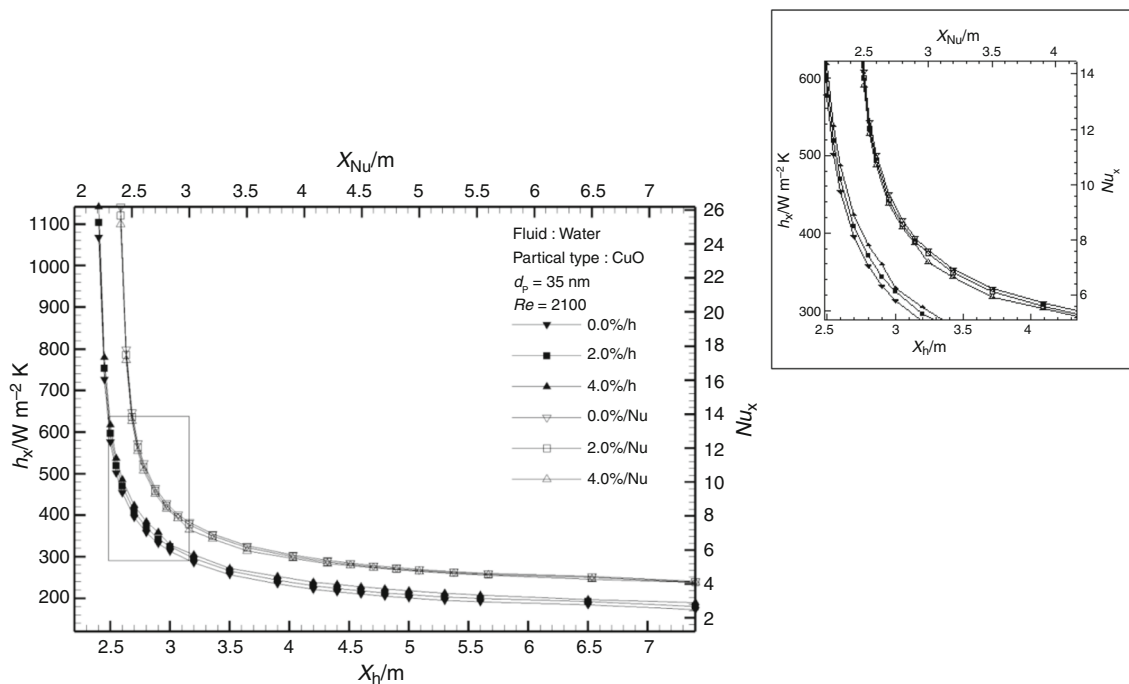

Fig. 21 Effect of volume fraction on heat transfer coefficient and local Nusselt number of water/CuO nanofluid at $Re = 2100$

and consequently heat transfer coefficient. Figure 25 shows local convective heat transfer coefficient and local Nusselt number at different diameters and volume fractions of nanoparticles at $Re = 2500$ for water/alumina nanofluid. The results show that local Nusselt number and local convective heat transfer coefficient slightly decrease with

increasing particle diameter at constant volume fraction of nanoparticles.

Figure 26 shows average convective heat transfer coefficient of water/alumina and water/CuO nanofluids versus volume fraction of nanoparticles at $Re = 2500$ and different diameters of nanoparticles. Similar to local charts, average heat transfer coefficient of nanofluid decreased
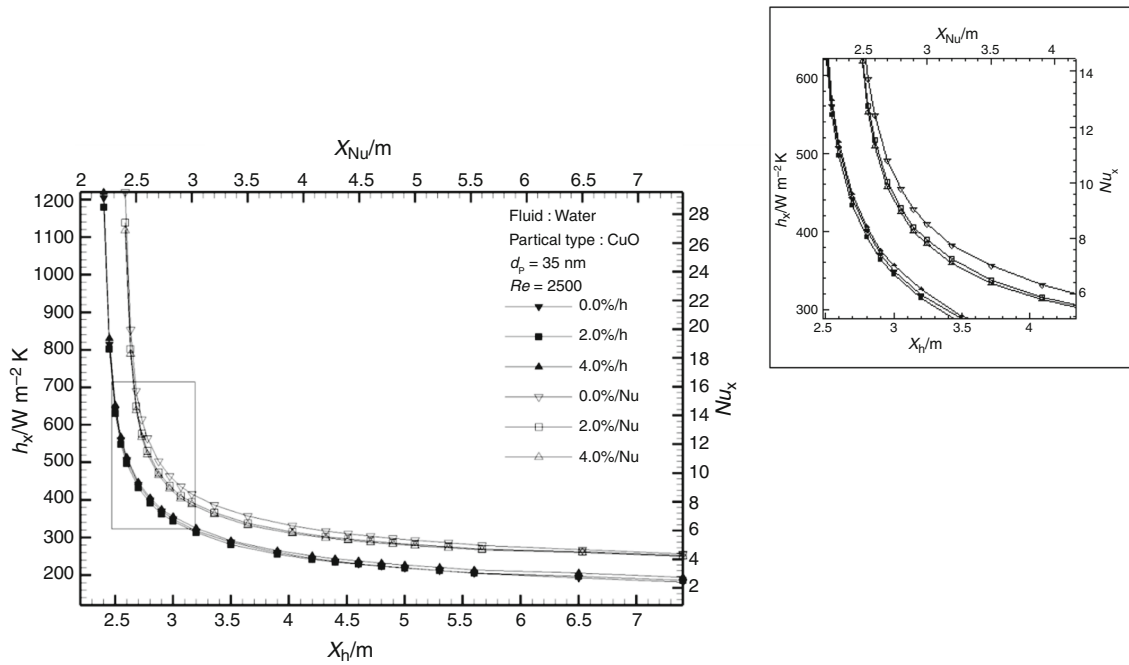
Fig. 22 Effect of volume fraction on heat transfer coefficient and local Nusselt number of water/CuO nanofluid at $Re = 2500$
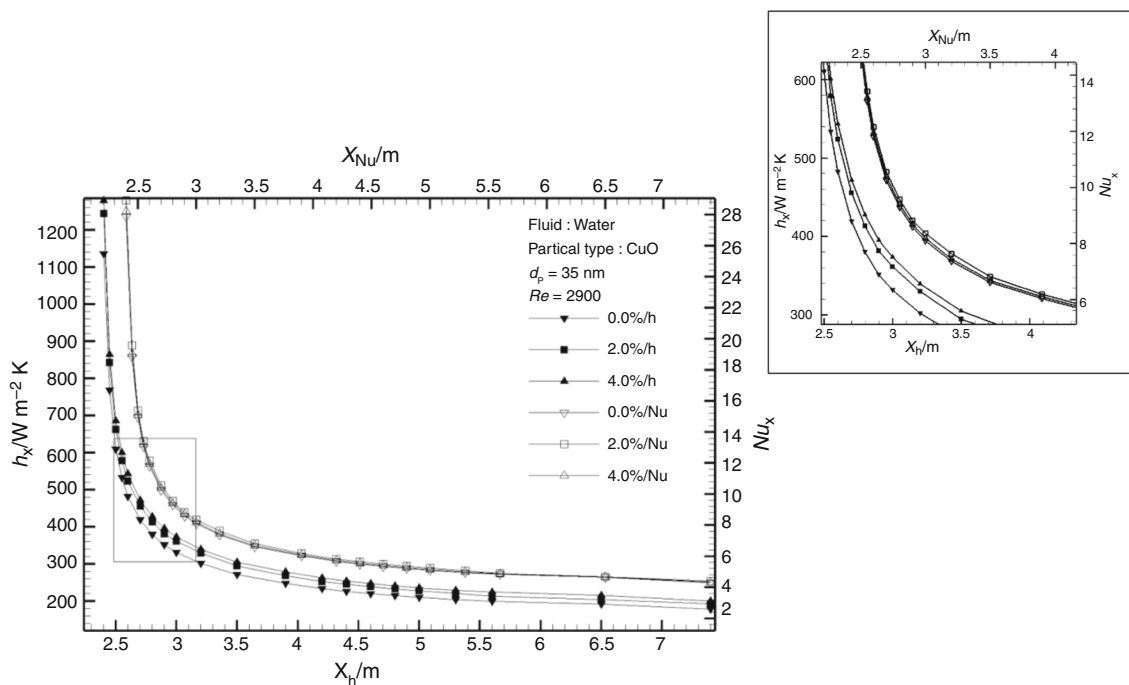

Fig. 23 Effect of volume fraction on heat transfer coefficient and local Nusselt number of water/CuO nanofluid at $Re = 2900$

with increasing particle diameter. For example, average heat transfer coefficients of water/alumina nanofluid decreased by 1.7% and 1.6% at 1% and 4% concentrations by increasing diameter of nanoparticles from 35 to 70 nm. Furthermore, average heat transfer coefficients of water/CuO nanofluid decreased by 1.77% and 1.65% at 1% and

4% concentrations by increasing the diameter of the particles from 35 to 70 nm. It seems that heat transfer coefficient further increases in both types of nanoparticles in the studied base fluid at low concentrations. However, decrease in average heat transfer coefficient induced by increase in nanoparticle diameter is compensated and made
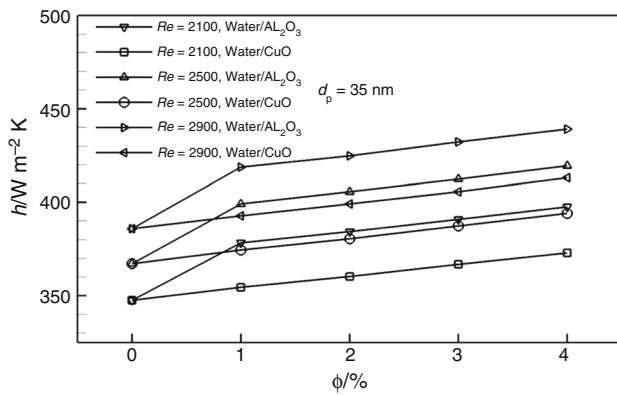
Fig. 24 Average convective heat transfer coefficient of water/CuO nanofluid and water/alumina nanofluid versus volume fraction of nanoparticles at 35 nm diameter and $Re = 2100$, 2500 and 2900

Fig. 26 Average convective heat transfer coefficient of water/alumina and water/CuO nanofluids versus volume fraction of nanoparticles at $Re = 2500$ and different diameters of nanoparticles

smaller by increasing volume fraction of nanoparticles. In addition, average heat transfer coefficient is further decreased in CuO compared to alumina.

Effect of nanoparticle type

Figure 27 shows local convective heat transfer coefficient and local Nusselt number of water fluid by changing both type and volume fraction of nanoparticles with 35 nm diameter at $Re = 2500$. Local charts show that heat transfer coefficient of water/alumina nanofluid is higher than water/CuO nanofluid at 1% volume fraction. The same trend was observed at 4% concentration. Type of nanoparticles is effective in nanofluid properties due to changes in thermal
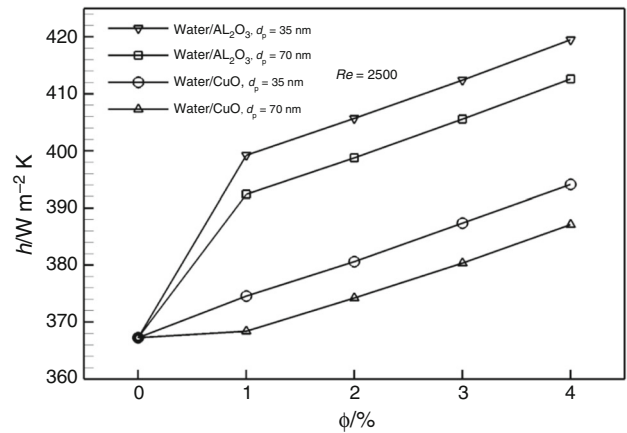
conductivity, density, specific heat and viscosity. Therefore, nanoparticle type is an effective parameter in heat transfer of nanofluids. Increased density increases the momentum and convection heat transfer. Mass flow rate increases at a constant velocity as fluid density increases. As a result, more fluid flows into the tube at unit mass flow rate and the fluid absorbs more heat from the wall. Moreover, increase in thermal conductivity accelerates heat transfer rate in the tube.

Figure 28 shows average convective heat transfer coefficient of water/alumina and water/CuO nanofluids versus Reynolds number in two different volume fractions and 35 nm diameter of nanoparticles. The difference in heat
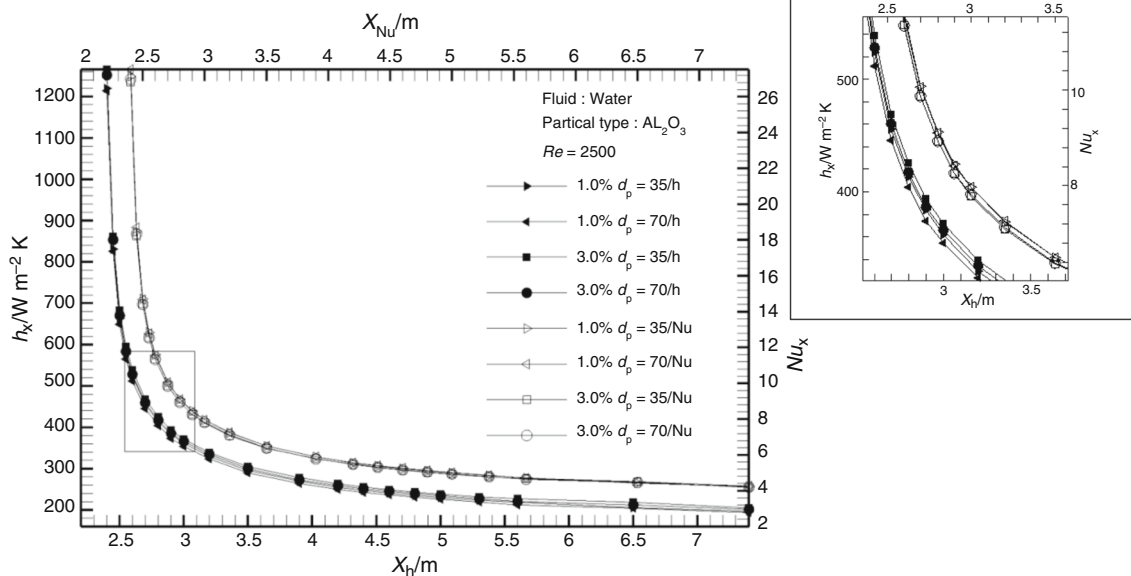

Fig. 25 Convective heat transfer coefficient and local Nusselt number with respect to changes in diameter and volume fraction of nanoparticles at $Re = 2500$ for water/alumina nanofluid
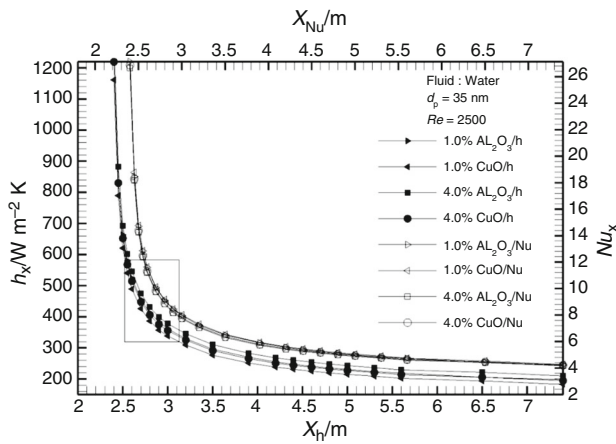
Fig. 27 Convective heat transfer coefficient and local Nusselt number of water fluid by changing both type and volume fraction of nanoparticles with 35 nm diameter at $Re = 2500$
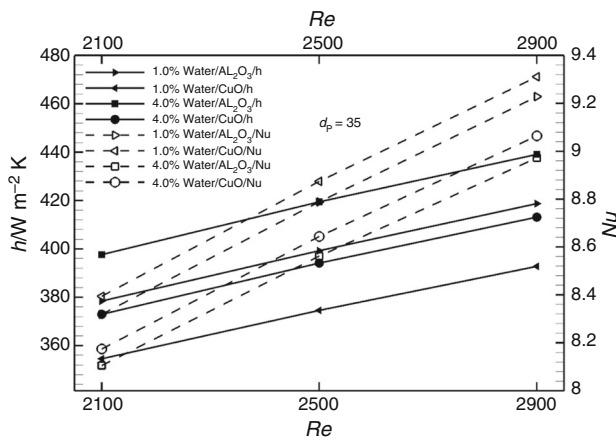

Fig. 28 Average convective heat transfer coefficient of water/alumina and water/CuO nanofluids versus Reynolds number in two different volume fractions and 35 nm diameter of nanoparticles

transfer coefficient of CuO and alumina is identical at 1% and 4% volume fractions. Convective heat transfer coefficients of alumina increased by 6.6%, 6.4% and 6.29% at $Re = 2100$, 2500 and 2900 and 4% volume fraction compared to CuO. This is because thermal conductivity of alumina is higher than CuO. It is also acknowledged that heat transfer coefficient of CuO nanofluid is more improved than coefficient of alumina with increasing Reynolds number at a constant volume fraction.

Conclusions

In this paper, we studied heat transfer characteristics in the developing and the developed flow of nanofluid inside a tube with different entrances in the transition regime. The following results were deduced by studying two different geometries:

1. Heat transfer coefficient and Nusselt number of base fluid and the nanofluid increased with increasing flow rate and consequently increasing the Reynolds number.
2. Convective heat transfer coefficient of CuO nanofluid increased by increasing Reynolds number.
3. The rate of increase in heat transfer coefficient varies depending on diameter and type of nanoparticle.
4. Convective heat transfer coefficient of CuO and alumina nanoparticles decreased with decreasing nanoparticle diameter.
5. Average heat transfer coefficients also decrease by 1.77% and 1.65% at 1% and 4% concentrations in water/CuO nanofluid by increasing nanoparticle diameter from 35 to 70 nm.
6. Heat transfer coefficient of CuO is lower than alumina. Period of changes in nanofluid with CuO is larger than alumina.
7. Heat transfer coefficient of CuO at 4% concentration was lower than alumina at 1% concentration.
8. The friction factor increased by increasing Reynolds number.
9. Surface friction factor does not depend on type and volume fraction of nanoparticles and follows the base fluid equation and increases with increasing Reynolds number.

References

1. Fung YC. Biomechanics—motion, flow, stress and growth. New York (USA): Springer; 1990. p. 569.
2. Manglik RM, Bergles AE. Heat transfer and pressure drop correlations for twisted-tape inserts in isothermal tubes: part 1—laminar flows. J Heat Transf. 1993;115:881–9.
3. Garcia A, Vicente PG, Viedma A. Experimental study of heat transfer enhancement with wire coil inserts in laminar-transition-turbulent regimes at different Prandtl numbers. Int J Heat Mass Transf. 2005;48:4640–51.
4. García A, Solana JP, Vicente PG, Viedma A. Enhancement of laminar and transitional flow heat transfer in tubes by means of wire coil inserts. Int J Heat Mass Transf. 2007;50:3176–89.
5. Tam LM, Ghajar AJ. Transitional heat transfer in plain horizontal tubes. Heat Transf Eng. 2006;27(5):23–38.
6. Tong Chong D, Liu J, Yan J. Effects of duct inclination angle on thermal entrance region of laminar and transition mixed convection. Int J Heat Mass Transf. 2008;51:3953–62.
7. Celata GP, Lorenzini M, Morini GL, Zummo G. Friction factor in micro pipe gas flow under laminar, transition and turbulent flow regime. Int J Heat Fluid Flow. 2009;30:814–22.
8. Lorenzini M, Morini GL, Salvigni S. Laminar, transitional and turbulent friction factors for gas flows in smooth and rough micro tubes. Int J Therm Sci. 2010;49:248–55.
9. Meyer JP, Olivier JA. Transitional flow inside enhanced tubes for fully developed and developing flow with different types of inlet

disturbances: part II—heat transfer. Int J Heat Mass Transf. 2011;54:1598–607.

10. Almohammadi H, Vatan SN, Esmaeilzadeh E, Motezaker A, Nokhosteen A. Experimental investigation of convective heat transfer and pressure drop of Al$_2$O$_3$/water nanofluid in laminar flow regime inside a circular tube. Int J Mech Aerosp Ind Mech Manuf Eng. 2012;6:1750–5.

11. Wang C, Gao P, Tan S, Wang Z. Forced convection heat transfer and flow characteristics in laminar to turbulent transition region in rectangular channel. Exp Therm Fluid Sci. 2013;44:490–7.

12. Heyhat MM, Kowsary F, Rashidi AM, Momenpour MH, Amrollahi A. Experimental investigation of laminar convective heat transfer and pressure drop of water-based Al$_2$O$_3$ nanofluids in fully developed flow regime. Exp Therm Fluid Sci. 2013;44:483–9.

13. Tam HK, Tam LM, Ghajar AJ. Effect of inlet geometries and heating on the entrance and fully-developed friction factors in the laminar and transition regions of a horizontal tube. Exp Therm Fluid Sci. 2013;44:680–96.

14. Karimzadehkhouei M, Eren Yalcin S, Sendur K, Mengu MP, Kosar A. Pressure drop and heat transfer characteristics of nanofluids in horizontal microtubes under thermally developing flow conditions. Exp Therm Fluid Sci. 2015;67:37–47.

15. Zeinali Heris S, Oghazian F, Khademi M, Saeedi E. Simulation of convective heat transfer and pressure drop in laminar flow of Al$_2$O$_3$/water and CuO/water nanofluids through square and triangular cross—sectional ducts. JREE. 2015;1:7–20.

16. Li Y, Seara JF, Du K, Pardinas AA, Latas LL, Jiang W. Experimental investigation on heat transfer and pressure drop of ZnO/Ethylene glycol-water nanofluids in transition flow. Appl Therm Eng. 2016;93:537–48.

17. Ebrahimnia-Bajestan E, Niazmand H, Duangthongsuk W, Wongwises S. Numerical investigation of effective parameters in convective heat transfer of nanofluids flowing under a laminar flow regime. Int J Heat Mass Transf. 2011;54:4376–88.

18. Pak BC, Cho YI. hydrodynamic and heat transfer study of dispersed fluids with submicron metallic oxide particles. Exp Heat Transf. 1998;11:151–70.

19. Xuan Y, Roetzel W. Conceptions for heat transfer correlation of nanofluids. Int J Heat Mass Transf. 2000;43:3701–7.

20. Garg J, Poudel B, Chiesa M, Gordon J, Ma J, Wang J. Enhanced thermal conductivity and viscosity of Copper nanoparticles in Ethylene glycol nanofluid. J Appl Phys. 2008;103:074301.

21. Chandrasekar M, Suresh S, Bose AC. Experimental investigations and theoretical determination of thermal conductivity and viscosity of Al$_2$O$_3$/Water nanofluid. Exp Therm Fluid Sci. 2010;34:210–6.

22. Vajjha RS, Das DK. Experimental determination of thermal conductivity of three nanofluids and development of new correlations. Int J Heat Mass Transf. 2009;52:4675–82.

23. Sundar LS, Singh MK. Convective heat transfer and friction factor correlations of nanofluid in a tube and with inserts: a review. Renew Sustain Energy Rev. 2013;20:23–35.

24. Meyer P, Liebenberg L, Olivier JA. Single-phase heat transfer and pressure drop of Water cooled inside horizontal smooth tubes in the transitional flow regime. In: 2010 14th International Heat Transfer Conference. 2010, pp 429–436.

25. Kim D, Kwon Y, Cho Y, Li C, Cheong S, Hwang Y. Convective heat transfer characteristics of nanofluids under laminar and turbulent flow conditions. Curr Appl Phys. 2009;9:119–23.

26. Mahian O, Kolsid L, Amani M, Estellé P, Ahmadi G, Kleinstreuer C, Marshall JS, Taylor RA, Abu-Nadal E, Rashidi S, Niazmand S, Wongwise S, Hayat T, Kasaeian A, Pop I. Recent advances in modeling and simulation of nanofluid flows-part I: fundamentals and theory. Phys Rep. 2019;790:2019.

27. Mahian O, Kolsid L, Amani M, Estellé P, Ahmadi G, Kleinstreuer C, Marshall JS, Taylor RA, Abu-Nadal E, Rashidi S, Niazmand S, Wongwise S, Hayat T, Kasaeian A, Pop I. Recent advances in modeling and simulation of nanofluid flows—part II: applications. Phys Rep. 2019;791:1–59.

28. Rezaei O, Akbari OA, Marzban A, Toghraie D, Pourfattah F, Mashayekhi R. The numerical investigation of heat transfer and pressure drop of turbulent flow in a triangular microchannel. Phys E. 2017;93:179–89.

29. Pourfattah F, Motamedian M, Sheikhzadeh Gh, Toghraie D, Akbari OA. The numerical investigation of angle of attack of inclined rectangular rib on the turbulent heat transfer of Water–Al$_2$O$_3$ nanofluid in a tube. Int J Mech Sci. 2017;131–132:1106–16.

30. Akbari OA, Karimipour A, Toghraie D, Safaei MR, Alipour Goodarzi MH, Dahari M. Investigation of Rib's height effect on heat transfer and flow parameters of laminar water–Al$_2$O$_3$ nanofluid in a two dimensional Rib-microchannel. Appl Math Comp. 2016;290:135–53.

31. Akbari OA, Toghraie D, Karimipour A. Numerical simulation of heat transfer and turbulent flow of Water nanofluids copper oxide in rectangular microchannel with semi attached rib. Adv Mech Eng. 2016;8:1–25.

32. Rahmati AR, Akbari OA, Marzban Ali, Toghraie D, Karimi R, Pourfattah F. Simultaneous investigations the effects of non-Newtonian nanofluid flow in different volume fractions of solid nanoparticles with slip and no-slip boundary conditions. Therm Sci Eng Prog. 2018;5:263–77.

33. Sarlak R, Yousefzadeh Sh, Akbari OA, Toghraie D, Sarlak S, Assadi F. The investigation of simultaneous heat transfer of water/Al$_2$O$_3$ nanofluid in a close enclosure by applying homogeneous magnetic field. Int J Mech Sci. 2017;133:674–88.

34. Gholami MR, Akbari OA, Marzban A, Toghraie D, Ahmadi Sheikh Shabani GHR, Zarringhalam M. The effect of rib shape on the behavior of laminar flow of oil/MWCNT nanofluid in a rectangular microchannel. J Therm Anal Calorim. 2018. https://doi.org/10.1007/s10973-017-6902-3.

35. Toghraie D, Mahmoudi M, Akbari OA, Pourfattah F, Heydari M. The effect of using water/CuO nanofluid and L-shaped porous ribs on the performance evaluation criterion of microchannels. J Therm Anal Calorim. 2019;1:2–3. https://doi.org/10.1007/s10973-018-7254-3.

36. Akbari OA, Afrouzi HH, Marzban A, Toghraie D, Malekzade H, Arabpour A. Investigation of volume fraction of nanoparticles effect and aspect ratio of the twisted tape in the tube. J Therm Anal Calorim. 2017;129(3):1911–22.

37. Arabpour A, Karimipour A, Toghraie D. The study of heat transfer and laminar flow of kerosene/multi-walled carbon nanotubes (MWCNTs) nanofluid in the microchannel heat sink with slip boundary condition. J Therm Anal Calorim. 2018;131(2):1553–66.

38. Esfahani NN, Toghraie D, Afrand M. A new correlation for predicting the thermal conductivity of ZnO–Ag (50%–50%)/water hybrid nanofluid: an experimental study. Powder Technol. 2018;323:367–73.